Electronic States and Potential Energy Surfaces of WC_2

Dingguo Dai and K. Balasubramanian*

Department of Chemistry and Biochemistry, Arizona State University, Tempe, Arizona 85287-1604

Received: October 7, 1999; In Final Form: December 1, 1999

Potential energy surfaces for the low-lying electronic states of the WC_2 molecule have been studied using the complete active space multiconfiguration self-consistent field (CASMCSCF) followed by the multireference singles + doubles configuration interaction (MRSDCI) calculations which include up to 3 million configurations. Spin−orbit effects are included through the relativistic configuration interaction (RCI) method. We find two nearly degenerate $^5B_1$ and $^3A_2$ electronic states for WC_2 both of which form stable minima with dissociation energy of 5.21 eV. Equilibrium geometries, energy separations, dipole moments, and the vibrational frequencies of the electronic states are reported. The nature of bonding is discussed using the wave function composition and the Mulliken population analysis. The spin−orbit effects were found to be quite significant.

I. Introduction

Driven by the importance of transition metal catalysts in reforming petroleum-based products, transition metal carbides have been studied intensely by several experimental and theoretical groups.[1−33] There has also been continued interest in spectroscopic and other studies of small transition metal carbides[1,3,5−16] varying from diatomic carbides (MC) to larger species. Larger transition metal carbon clusters such as metallofullerenes[2], metallocarbohedranes, and unusually stable "metcars"[32] have been the topic of many studies. The nature of transition metal−carbon bond remains a puzzle, despite many studies, due to the complex bonding in these species and the interesting interplay among the electron correlation energy, spin exchange energy, and relativistic effects.[34]

Early experimental studies on transition metal carbides have employed the Knudsen effusion technique combined with mass spectrometry,[4−7] which have yielded atomization energies and related properties of these species. More recently, the state-of-the-art experimental techniques such as the ion drift tube technique,[1,9−11] electron spin resonance spectra[14−16] of carbides isolated in rare gas matrixes, and high-resolution optical spectroscopy[12,13] have been employed to study transition metal carbides ranging from diatomics to more complex $LaC_n^{+\ 1}$ and $TaC_n^{+\ 3,33}$ for several values of *n*.

While several transition metal carbides containing La, Y, Fe, Co, Nb, Rh, Ta, Pd, etc. have been studied,[17−31] there are no comparable experimental or theoretical studies on tungsten-containing carbides. Yet as we show here tungsten carbides are very strongly bound and have rich low-lying electronic states and are thus very promising species for future experimental studies.

Theoretical studies of transition metal carbides are challenging due to the possibility of a large array of electronic states of varying spin multiplicities and geometries. The relative ordering of electronic states of different spin multiplicities tend to change as a function of level of theory due to large electron correlation effects which have complex many-body character in their contributions to different states. Often an electronic state, which is determined to be the ground state at a lower level of theory becomes an excited state at a higher level of theory, since electron correlation contributions tend to differ for different states. This is further complicated by large relativistic effects[34] for heavier species such as tungsten carbides since relativistic effects and electron correlation effects couple for such systems resulting in different characteristics. Tungsten carbides are very interesting in this regard because even the ground state of the tungsten atom differs with and without relativistic effects.[41] We note that although WC_2 has not been studied before theoretically, Pyykkö and Tamm[42] have studied the related WN_2 molecule.

The objective of the current study is systematic computation of the potential energy surfaces, equilibrium geometries, and spectroscopic properties of the triatomic WC_2 molecule. We investigate several possible low-lying electronic states at the CASSCF and MRSDCI levels that included up to 3 million configurations. We also include spin−orbit effects using a relativistic configuration interaction (RCI) scheme.

II. Method of Calculation

We employed relativistic effective core potentials (RECPs) for the W atom taken from Ross et al.,[35] which retained the outer $5s^25p^65d^46s^2$ shells for the tungsten atom in the valence space replacing the remaining core electrons by RECPs. The RECPs for the carbon atom retained the outer $2s^22p^2$ shells in the valence space. The optimized valence (5s5p4d) Gaussian basis sets for the W atom were taken from ref 35. We started with the (5s5p4d) basis sets, which were contracted to (5s3p3d) basis sets. The first three (large exponents) p functions and first two d functions were contracted. The contracted p functions represent the core 5p orbitals, and thus the contraction should have negligible impact on the valence electronic properties considered in this investigation. The (4s4p) optimized Gaussian basis sets for the carbon atoms were contracted to (3s3p). The carbon basis sets were supplemented with a set of six-component 3d functions with $\alpha_d = 0.75$. Our final basis sets are (5s3p3d) for the tungsten atom and (3s3p1d) for the carbon atoms. In a previous investigation on WCO,[41] we have studied the effect of 4f functions. It was found that the inclusion of 4f functions changes the W−C bond lengths by 0.01 Å and bond relative

* To whom correspondence should be addressed. E-mail: kbalu@asu.edu.

10.1021/jp993587g CCC: $19.00
Published on Web 01/20/2000

energy separations by 0.01−0.1 eV. We found the effect of spin−orbit coupling to be far more important than the effect of 4f functions. Hence, in the present study, 4f functions were not included in the basis set.

The WC_2 molecule was computed in the C_{2v} point group placing the molecule on the *yz* plane and the *z*-axis chosen as the C_2 axis. The orientation of the molecule is relevant to describe the orbitals and the active space. We carried out separate CASMCSCF calculations for electronic states of different spatial symmetries and spin multiplicities in the C_{2v} point group. The C−W−C apex angles were varied from 20° to 180°. For each apex angle, the two equal sides of the isosceles triangle were optimized.

The four orbitals that correspond to the 5s and 5p orbitals of the tungsten atom were kept inactive in the sense that no excitations from these shells were allowed, but these orbitals were allowed to relax. Among the remaining high-lying orbitals, five a_1, three b_2, two b_1, and one a_2 orbitals (C_{2v} group) were included in the active space. In all, 14 valence electrons were distributed in all possible ways among these active orbitals. This choice of active and inactive spaces can be labeled as $n_a = 5$, 3, 2, 1 (a_1, b_2, b_1, a_2) and $n_i = 2$, 1, 1, 0. Separate CASMCSCF calculations were carried out for 12 singlet, triplet, and quintet electronic states. The CASMCSCF computations included up to 12 758 configuration spin functions (CSFs).

Following the CASMCSCF calculations, the MRSDCI calculations were carried out for all 12 singlet, triplet, and quintet electronic states of WC_2 to include the effects of higher-order electron correlation. Single and double excitations of 14 electrons from a chosen set of reference configurations into all of the external orbitals were allowed at the MRSDCI stage. The reference configurations for the MRSDCI computations were chosen from the preceding CASMCSCF calculations with absolute coefficients of ≥ 0.07. We also carried our MRSDCI computations with reference configurations with absolute coefficients of ≥ 0.05 for the nearly degenerate $^3A_2$ and $^5B_1$ electronic states to gauge the effect of higher order electron correlation effects on the relative ordering of the states. The MRSDCI computations included up to 3 million configuration spin functions (CSFs).

We computed the vibrational frequencies of the $^5B_1$ state at the density functional level of theory (DFT) using the B3LYP correlation-exchange potentials.[43] For this purpose, we started with spin unrestricted Hartree−Fock (UHF) computation of this state followed by UB3LYP geometry optimization and frequency computation. The UB3LYP computations were made with the Gaussian 98 codes.[44]

Following the MRSDCI calculations, the relativistic configuration interaction (RCI) calculations[36] that included low-lying electronic configurations of different spatial and spin symmetries in the presence of the spin−orbit operator were carried out to estimate the spin−orbit contributions. Our RCI calculations carried out in the double group included all of the open-shell spin combinations that arise from different electronic states. This resulted in 51 reference configurations for the A_1 state (C_{2v}^2 double group) and 50 reference configurations for each B_1, B_2, and A_2 spin−orbit state. We chose seven a_1 orbitals, five b_2 orbitals, three b_1 orbitals, and two a_2 orbitals as the active space, where 12 electrons were allowed for excitation and interaction. Single and double excitations from these reference configurations were included in the RCI computations.

All CASMCSCF/MRSDCI calculations were made using a modified version of ALCHEMY II codes[38] to include the RECPs. The spin−orbit integrals derived from the RECPs using

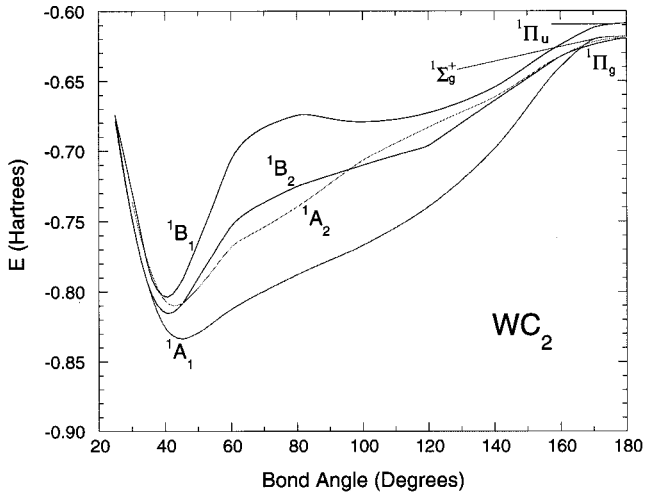

Figure 1. Potential energy curves for the singlet states of WC_2.

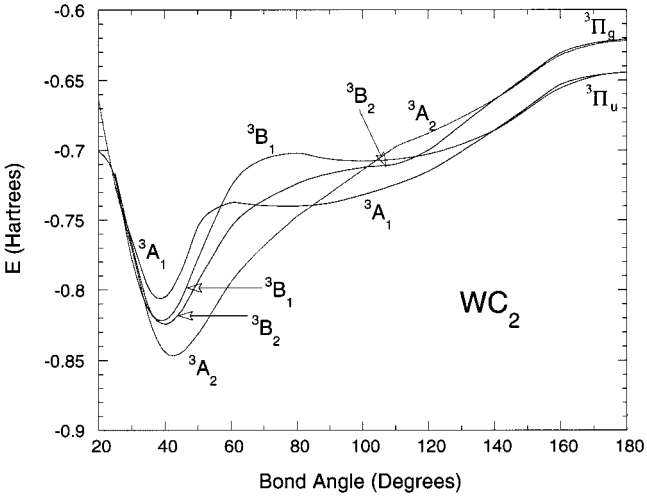

Figure 2. Potential energy curves for the triplet states of WC_2.

Pitzer's ARGOS[37] codes were transformed in the MRSDCI natural orbitals obtained in the absence of spin−orbit coupling. These integrals were added to the CI Hamiltonian matrix and the computations were carried out in the double group[34] according to the procedure described earlier.

III. Results and Discussion

Figures 1−3 show the CASMCSCF potential energy surfaces for the singlet, triplet and, quintet electronic states of WC_2, respectively, as a function of the C−W−C apex angles. For each apex angle, the W−C sides of the isosceles triangle were optimized and the optimized energy is plotted in the figures. Table 1 shows the actual equilibrium geometries, and the relative energy separations of the bound electronic states of WC_2 at both CASMCSCF and MRSDCI levels.

It is evident from our computations that there are two nearly degenerate electronic states with isosceles triangular structures, namely a $^5B_1$ state, which is the ground state at the CASSCF level, but the $^3A_2$ state becomes a very viable candidate for the ground state at higher MRSDCI and MRSDCI+Q levels. Although at the CASMCSCF level the $^3A_2$ state was found to be 0.20 eV higher than the $^5B_1$ state, it is only 0.04 eV higher at the MRSDCI level. When we include the unlinked quadruple cluster correction, the $^3A_2$ state is stabilized by 0.14 eV compared to the $^5B_1$ state. This clearly reveals that higher-order electron correlation effects tend to stabilize the low-spin $^3A_2$

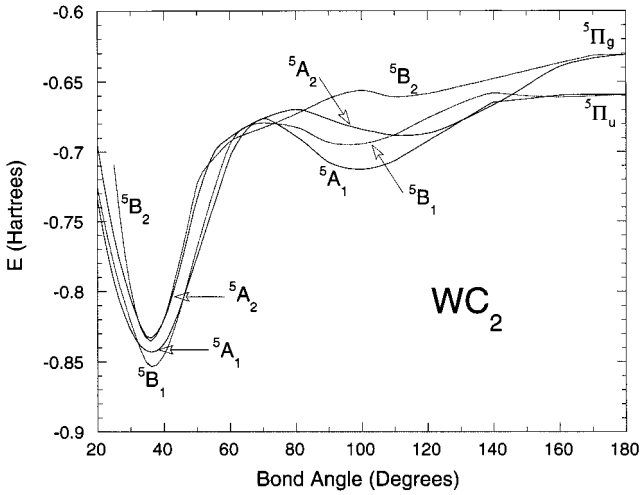

Figure 3. Potential energy curves for the quintet states of WC_2.

TABLE 1: Geometries and Energy Separations of Electronic States of WC_2

	CASMCSCF				MRSDCI			
state	θ (deg)[a]	W−C (Å)	C−C (Å)	E (eV)	θ (deg)[a]	W−C (Å)	C−C (Å)	E (eV)[b]
$^5B_1$	36.7	2.056	1.295	0.00	37.8	2.024	1.311	0.00 (0.00)
$^3A_2$	42.6	1.916	1.392	0.20	45.2	1.873	1.439	0.04 (−0.14)
$^5A_1$	36.2	2.066	1.284	0.28	37.8	2.020	1.309	0.28 (0.09)
$^5B_2$	35.8	2.065	1.269	0.48	35.7	2.068	1.268	0.82 (0.91)
$^1A_1$	45.6	1.868	1.448	0.54	49.8	1.817	1.530	1.12 (0.74)
$^5A_2$	35.8	2.088	1.284	0.53	36.4	2.073	1.295	1.35 (1.33)
$^3B_2$	40.3	1.935	1.333	0.79	43.6	1.871	1.390	0.77 (0.36)
$^3B_1$	39.1	1.966	1.316	0.86	41.0	1.922	1.346	0.75 (0.43)
$^1B_2$	41.3	1.918	1.353	1.03	44.3	1.861	1.404	1.02 (0.71)
$^1A_2$	43.1	1.903	1.398	1.20	45.9	1.863	1.452	0.95 (0.73)
$^3A_1$	38.8	1.983	1.317	1.29	40.1	1.950	1.337	1.29 (1.07)
$^1B_1$	40.6	1.923	1.334	1.35	41.6	1.906	1.354	1.28 (0.98)

[a] θ stands for C−W−C apex angle. [b] The values in parentheses are Davidson corrected energies.

state. Consequently, we suggest that the $^3A_2$ state as the most probable ground state of WC_2. It may also be seen from Table 1 that the $^5A_1$ state is close to the $^3A_2$ state.

As evidenced from Table 1, although the CASMCSCF method yields reasonable geometries, it is less accurate, especially with respect to energy separations, as it does not include dynamical electron correlation effects, which tend to have substantial impact on energy separations. As seen from Table 1, in addition to the states discussed above, for example, the $^3B_1$ and $^3B_2$ states are higher than the $^5A_2$ state by 0.26−0.33 eV at the CASMCSCF level, but at the MRSDCI level, the $^3B_1$ and $^3B_2$ states were 0.58−0.60 eV lower than the $^5A_2$ state. These states are even more stabilized at the MRSDCI + Q level in that the $^3B_1$ and $^3B_2$ states are found to be 0.90−0.97 eV lower than the $^5A_2$ state at this level.

The $^1B_2$, $^1A_2$, and $^1B_1$ states are higher than the $^5B_1$ state by at least an electronvolt at the CASMCSCF level. Among the singlet states, only the $^1A_1$ state exhibits a low-lying minimum which is 0.54 eV higher than the lowest electronic state of WC_2.

The potential energy surfaces of the electronic states of WC_2 (Figures 1−3) exhibit several interesting features. First, all of the electronic states of WC_2 exhibit very acute apex angles between 35° and 46°. This is suggestive of short C−C bonds in addition to strong W−C bonds, and since C−C bonds have relatively shorter bond lengths compared to the W−C bonds, all of the equilibrium structures are isosceles triangular structures. As seen from Table 1, higher order electron correlation effects enlarge the C−W−C apex angles up to 4.2° for most of the states due to stabilization of the W−C bonds.

TABLE 2: Properties of the Saddle Points and the Local Minima of Some Bent States of WC_2 at the CASMCSCF Level

	saddle points			local minima[a]		
state	θ (deg)[b]	W−C (Å)	E (eV)	θ (deg)[b]	W−C (Å)	E (eV)
$^5B_1$	75.2	1.846	4.70	96.4	1.842	4.32
	136.8	1.871	5.03	180.0	1.897	4.65
$^5A_1$	72.2	1.844	4.87	99.4	1.821	3.84
$^5A_2$	82.2	1.904	5.01	112.2	1.832	4.49
$^5B_2$	101.5	1.860	5.38	111.6	1.865	5.24
$^3B_1$	81.0	1.831	4.13	100.3	1.826	3.97
$^3A_1$	63.8	1.788	3.20	76.6	1.777	3.09
$^1B_1$	87.2	1.822	4.93	98.6	1.823	4.72

[a] The equilibrium geometry and the corresponding minimum of the energy which appear in Table 1 will not be listed here again. [b] θ stands for C−W−C apex angle.

As seen from Figure 3, a remarkable common feature to all of the quintet electronic states is that they form a double minima separated by a saddle point. For example, the $^5B_1$ state exhibits prominent double minima at apex bond angles of 36.7° and 96.4°, respectively. However, as seen from Table 2, these local minima are substantially higher in energy (4.3−5.2 eV at the MRSDCI level). We also found two saddle points in the potential energy curves of the $^5B_1$ state at apex bond angles of 75.2° and 136.8°. As seen from Table 2, two triplet electronic states and a singlet electronic state exhibit local minima and saddle points. The multiple minima are attributed to avoided curve crossings that will be discussed in a subsequent section.

The vibrational frequencies were computed using the density functional level of theory in conjunction with the B3LYP potentials. The A_1 symmetric stretch vibrational frequency was computed as 1607 cm^{-1}, while the B_2 asymmetric and A_1 bending modes frequencies were computed as 571 and 584 cm^{-1}, respectively. The B3LYP optimized geometry for the $^5B_1$ state is an isosceles triangle with an apex angle of 38.25°, a W−C bond length of 2.001 Å, and a C−C bond distance of 1.311 Å. This geometry is close to the MRSDCI equilibrium geometry for the $^5B_1$ state in Table 1.

We calculated the dissociation energy to separate WC_2 into W and C_2. At the CASMCSCF level, we computed the dissociation energy (D_e) as 4.16 eV, while at the higher MRSDCI and MRSDCI+Q levels this value becomes 5.21 and 5.22 eV, respectively. The experimental D_e of C_2 is well established as 6.21 eV.[40] The D_e of C_2 was computed with our basis set as 6.07 eV at the CASSCF level and 5.95 eV at the second-order CI (SOCI) level. If we combine our computed D_e of WC_2 with the experimental D_e of C_2, we obtain the atomization energy of WC_2 as 11.4 eV. On the other hand, when the D_e of WC_2 is combined with our theoretical (SOCI) D_e we obtain the atomization energy of WC_2 as 11.2 eV. The zero-point correction for WC_2 is computed as 0.145 eV.

Table 3 shows the effect of spin−orbit coupling on the low-lying electronic states of WC_2 as computed using the RCI method which included both electron correlation and spin−orbit effects. As seen from Table 3, the $^5B_1$ ground state without the spin-effect was split into the $^5B_1(B_1)$, $^5B_1(B_2)$, $^5B_1(A_1)$, and $^5B_1(A_2)$ states in the double group when spin−orbit effects are included. Among these states, the $^5B_1(B_1)$ state was found to be the ground state. This relativistic state is composed of 94% $^5B_1$ and small contributions (2%) from the $^3A_2$, $^5A_2$, $^3B_2$, and $^5B_2$ states. As a consequence of small spin−orbit contamination, as seen from Table 3, the geometries do not change too much

TABLE 3: Properties of the Bent States of WC_2 Including Spin−Orbit Effects

	θ (deg)[a]		W−C (Å)		E (cm^{-1})		weights (%)						
state	SO	no SO	SO	no SO	SO	no SO	$^5B_1$	$^1A_1$	$^3A_2$	$^5A_1$	$^5A_2$	$^3B_2$	$^5B_2$
$^5B_1(B_1)$	37.7	37.8	2.031	2.024	−634	0	94		0.7		0.1	0.8	0.2
$^5B_1(B_2)$	37.6	37.8	2.033	2.024	−593	0	97		0.5		0.2		0.3
$^5B_1(A_1)$	37.8	37.8	2.027	2.024	−540	0	93		0.3	0.5	0.1	1.6	0.2
$^5B_1(A_2)$	37.9	37.8	2.023	2.024	1240	0	93		0.7	0.4	0.3	2.1	0.8
$^1A_1(A_1)$	49.6	49.8	1.820	1.817	8386	8996		94	0.1	1.5		1.6	

TABLE 4: Dipole Moments of the Electronic States of WC_2[a]

state	μ_e (debye)	state	μ_e (debye)
$^5B_1$	5.721	$^3B_2$	3.167
$^3A_2$	7.072	$^3B_1$	4.199
$^5A_1$	4.932	$^1B_2$	4.077
$^5B_2$	5.778	$^1A_2$	5.861
$^1A_1$	6.588	$^3A_1$	4.324
$^5A_2$	5.653	$^1B_1$	2.921

[a] Positive polarity means W^+C^- polarity and the dipole vector is in the $+z$ direction.

when the spin effects are included but the ground electronic state is split by 1875 cm^{-1}. The $^5B_1(B_1)$, $^5B_1(B_2)$, and $^5B_1(A_1)$ states are stabilized by 634, 593, and 540 cm^{-1}, respectively, while the $^5B_1(A_2)$ spin−orbit state is destabilized by 1240 cm^{-1} compared to the $^5B_1$ state without the spin-effect. The magnitude of the spin−orbit effect is determined by the extent of participation of the W atom in the appropriate open-shell orbitals in the electronic state under consideration. It is also interesting to note that even though the $^1A_1$ state is a closed-shell state, the open-shell $^3B_2$ and $^5A_1$ states make small contributions (3.1%) to this closed-shell state.

Table 4 shows the dipole moments of the low-lying electronic states of WC_2 at their equilibrium geometries. As seen from Table 4, the electronic states of WC_2, regardless of their spin multiplicites, exhibit large dipole moments consistent with their ionic bonding characterized by charge transfer from W to the carbon atoms and smaller dative back transfer from the carbon atoms to W. Both $^5B_1$ and $^3A_2$ states exhibit comparable dipole moments. The polarity of the W−C bonds are W^+C^- and the overall dipole vector points in the $+z$ direction relative to the orientation of the molecule, which is on the *yz* plane with the *z* axis bisecting the C−W−C apex angle. The large dipole moments of the electronic states of WC_2 are also consistent with very acute apex angles exhibited by these states. Generally, as the bond angle increases, the dipole moment decreases for a given amount of charge transfer due to the vectorial nature of the dipole moment. It should be mentioned that the MRSDCI dipole moments reported in Table 4 have reasonable accuracy with respect to electron correlation effects. For example, the dipole moment of the $^5B_1$ state is computed as 2.300 au (1 au = 2.5418 D) at the MRSDCI level that included all reference configurations with absolute coefficients of ≥ 0.07, while the MRSDCI that included all configurations with absolute coefficients of ≥ 0.05 (rounded) yielded the dipole moment to be 2.275 au. Consequently, the reported dipole moments are converged relative to electron correlation effects but further improvements in the basis sets may have small influence on these values.

IV. The Bonding Nature of the Low-Lying States of WC_2

The nature of bonding of transition metal containing species is quite complex due to the participation of not only the 6s and 5d orbitals but also the 6p orbital of the W atom. Moreover, there is charge transfer from the W atom to the carbon atoms and back transfer from the carbons to the W atom. Consequently, to assist in providing insight into the nature of bonding, we consider the leading configurations, Mulliken populations, and compositions of the higher orbitals.

TABLE 5: Leading Configurations of the Electronic States of $W-C_2$ in the MRSDCI Wave Function[a]

		configurations				
state	coefficient	$6a_1$	$7a_1$	$3b_2$	$3b_1$	$1a_2$
$^5B_1$	−0.91	1	1	1	0	1
$^3A_2$	−0.89	1	0	2	0	1
$^5A_1$	−0.90	1	0	1	1	1
$^5B_2$	−0.92	1	1	0	1	1
$^1A_1$	0.90	0	0	2	0	2
$^5A_2$	−0.92	1	1	1	1	0
$^3B_2$	0.89	1	0	1	0	2
$^3B_1$	0.89	2	0	1	0	1
$^1B_2$	0.89	1	0	1	0	2
$^1A_2$	0.90	1	0	2	0	1
$^3A_1$	−0.76,−0.37,−0.25	1	0	1	1	1
$^1B_1$	−0.88	2	0	1	0	1

[a] The $(1a_1)^2 \ldots (5a_1)^2(1b_2)^2(2b_2)^2(1b_1)^2(2b_1)^2$ is common to all the electronic states.

Table 5 shows the leading configurations and their coefficients for the low-lying electronic states of WC_2 in the MRSDCI wave functions. Generally, almost all of the electronic states of WC_2 are predominantly composed of a single configuration with coefficients of >0.88, the only exception being the $^3A_1$ state, but the three-configuration spin functions contributing to this state originate from the same electronic occupancies. It may also be useful to analyze the configurations of the excited states relative to the $^5B_1$ state. Thus, the $^3A_2$ state arises from the promotion of an electron from the $7a_1$ orbital to the $3b_2$ orbital relative to the $^5B_1$ state. On the other hand, as seen from Table 5, the $^5A_1$ state arises from the excitation of the $7a_1$ electron to the $3b_1$ orbital. Likewise, some states involve promotion of $3b_2$ to $3b_1$ or to $1a_2$. Consequently, the compositions of the $6a_1$, $7a_1$, $3b_2$, $3b_1$, and $1a_2$ orbitals shown in Table 5 are analyzed.

The singly occupied $3b_2$ orbital of the $^5B_1$ state is mainly composed of $W(5d_{yz}) + C_1(2s) - C_2(2s)$, but the $C_1(2p_z) - C_2(2p_z)$ orbital and $W(6p_y)$ also make small contributions. The singly occupied $6a_1$ orbital is composed of W(6s), $W(5d_{x^2+z^2-2y^2})$, W $(5d_{x^2-z^2})$, $W(6p_z)$, and $C_1(2p_y) - C_2(2p_y)$, where the W(6s) makes a slightly larger contribution. The $7a_1$ orbital is composed of $W(5d_{x^2+z^2-2y^2})$ and $W(5d_{x^2-z^2})$, with small mixing from W(6s) but practically no contributions from the carbons atoms. The lowest unoccupied $3b_1$ orbital is composed primarily of $W(5d_{xz}) + C_1(2p_x) + C_2(2p_x)$ with small contribution from $W(6p_x)$. The $1a_2$ orbital is primarily nonbonding $W(5d_{xy})$ orbital.

Since the orbitals are somewhat complex, we have shown plots of the four highest doubly occupied orbitals in Figure 4 and highest singly occupied orbitals in Figure 5. These figures provide further insight into the nature of these orbitals. The orbitals plotted in these figures are for the $^5B_1$ ground state near its global minimum.

The double minima in the potential energy surface of the $^5B_1$ state (See Figure 3 and Table 2) arise from avoided crossings. At a C−W−C apex angle of 60°, the $^5B_1$ state is predominantly

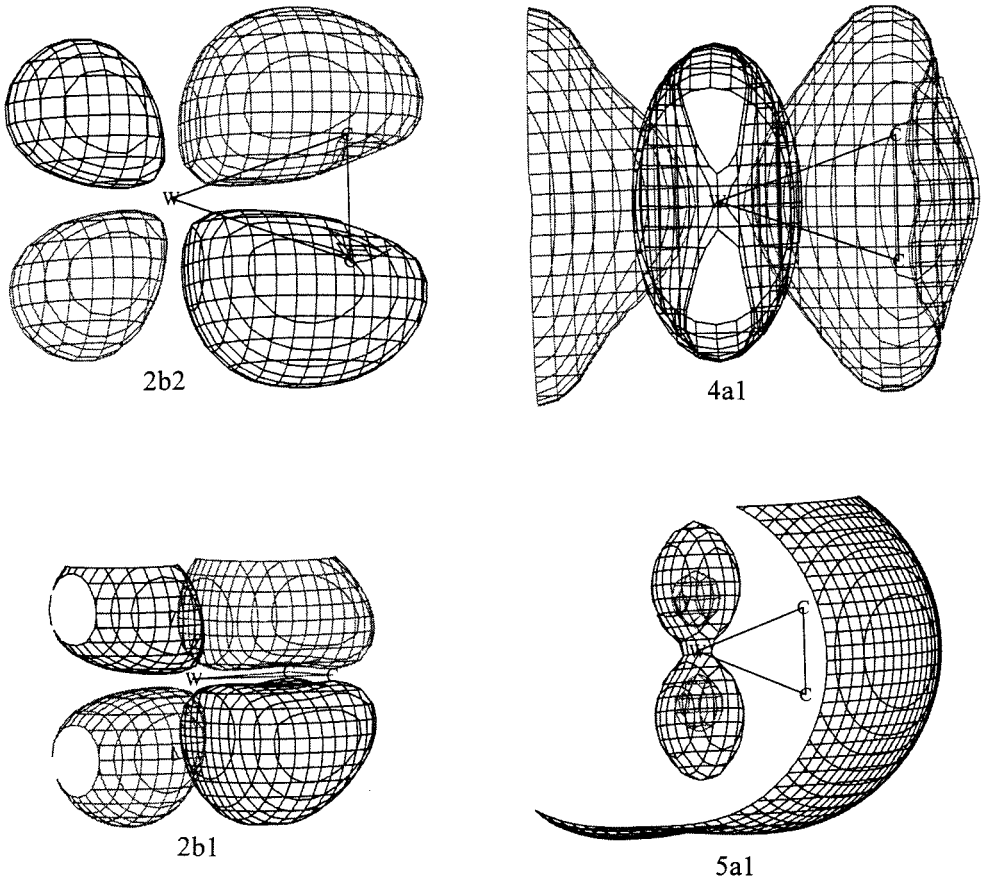

Figure 4. Plots of the highest doubly occupied orbitals of WC_2 in the $^5B_1$ state.

composed of $(1a_1)^2 \ldots (5a_1)^2(1b_2)^2(2b_2)^2(1b_1)^2(2b_1)^2(6a_1)^1(7a_1)^1(3b_2)^1(1a_2)^1$ (coefficient, 0.92), while at a C−W−C apex angle of 80° it is made of $(1a_1)^2 \ldots (4a_1)^2(1b_2)^2(2b_2)^2(3b_2)^2(1b_1)^2(2b_1)^2(5a_1)^1(6a_1)^1(4b_2)^1(1a_2)^1$ (coefficient, 0.89). At a C−W−C apex angle of 140° it is made of $(1a_1)^2 \ldots (4a_1)^2(1b_2)^2(2b_2)^2(3b_2)^2(1b_1)^2(1a_2)^2(5a_1)^1(6a_1)^1(7a_1)^1(4b_2)^1$ (coefficient, 0.85). These avoided crossings in the $^5B_1$ state result in the double minima and the saddle point in the potential surface in Figure 3.

The geometries of the electronic states are determined by their leading configurations and the orbital compositions of the leading configurations. If the overall compositions of two electronic states are nearly same, their apex bond angles are also similar. For example, the leading configurations and orbital compositions of the $^3B_1$ and $^1B_1$ states are quite similar, as seen from Table 5. Thus, their equilibrium bond angles are 41.0° and 41.6°, respectively (Table 1). Also, both $^3B_1$ and $^1B_1$ states have saddle points (Table 2). However, the $^5B_1$ ground state has two singly occupied $6a_1$ and $7a_1$ orbitals instead of a doubly occupied $6a_1$ orbital for the $^3B_1$ and $^1B_1$ states, and hence its apex bond angle differs substantially to 37.8° at the MRSDCI level.

The Mulliken population analysis in Table 6 indicates the involvement of tungsten and carbon orbitals and electron transfer in the bonding of WC_2. As seen from Table 6, for all electronic states we investigated in this study, the apex tungsten atom has a Mulliken population between 5.43 and 5.74, while each of the two carbon atoms has a gross population between 4.13 and 4.29. This indicates electron transfer from the tungsten atom to the carbon atoms. The 6s populations of the tungsten atom for all electronic states are between 0.68 and 1.44, while the 5d populations are more than 4.0 with the exception of the $^3B_1$ and $^5A_2$ states, which have 4d populations very close to 4.0. The 6p populations of the tungsten atom are between 0.13 and 0.47. All of these features suggest that the W atom does not exist in a pure atomic form but it exhibits significant 6p and reduced 6s character. The reduction in the 5d and 6s participation is both due to charge transfer to carbons and the 6p participation. It is thus evident that the tungsten atom exhibits a 5d6s6p hybrid character. For the carbon atoms, all 2s orbitals have populations less than 1.84, while the 2p populations are more than 2.39. The variations from their pure atomic populations are both due to hybridization and charge transfer from W.

TABLE 6: Mulliken Population Analysis for the Electronic States of WC_2[a,c]

	gross population						
state	W	C[b]	W(s)	W(p)	W(d)	C(s)[b]	C(p)[b]
$^1A_1$	8.430	4.285	0.683	0.127	4.620	1.838	2.388
$^1B_2$	8.624	4.188	1.032	0.232	4.360	1.603	2.525
$^1B_1$	8.736	4.132	1.418	0.272	4.046	1.524	2.547
$^1A_2$	8.482	4.259	0.901	0.197	4.384	1.777	2.422
$^3A_1$	8.526	4.237	0.700	0.472	4.354	1.540	2.639
$^3B_2$	8.616	4.192	1.011	0.244	4.361	1.615	2.516
$^3B_1$	8.708	4.146	1.437	0.286	3.985	1.568	2.517
$^3A_2$	8.470	4.265	0.822	0.194	4.454	1.780	2.425
$^5A_1$	8.495	4.253	0.728	0.395	4.372	1.604	2.593
$^5B_2$	8.487	4.256	0.879	0.426	4.182	1.555	2.645
$^5B_1$	8.548	4.226	0.965	0.282	4.301	1.691	2.476
$^5A_2$	8.462	4.269	1.028	0.452	3.982	1.633	2.581

[a] The $5s^25p^6$ shells for W are excluded from the Mulliken populations. [b] Represents one of the two equivalent C atoms. [c] The d and s populations were corrected for $d(x^2 + y^2 + z^2)$ term.

It can be seen from Table 6 that the $^5B_1$ state for WC_2 is composed of $W(5d^{4.301}6s^{0.965}6p^{0.282})$ and $C(2s^{1.691}2p^{2.476})$. Since the quintet states arise from the $W(5d^46s^2)^5D$ atom, populations can be compared with this state to deduce the extent of charge transfer and hybridization. In the $^5B_1$ state, carbon transfers

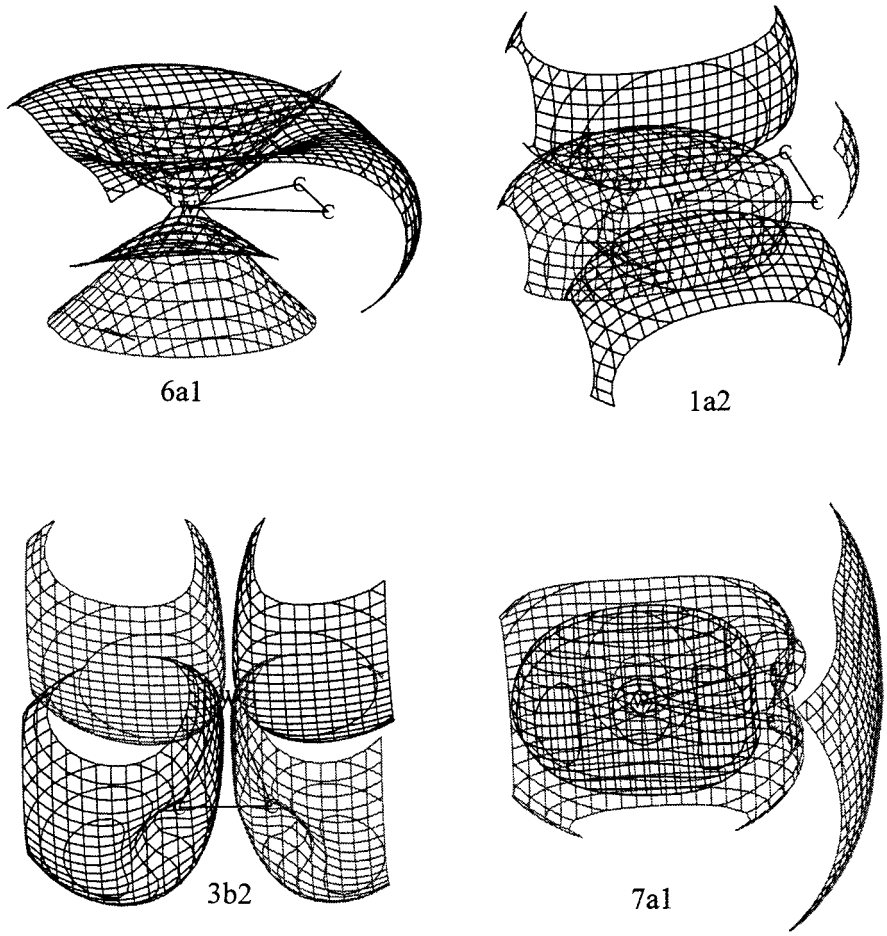

Figure 5. Plots of the highest singly occupied orbitals of WC_2 in the $^5B_1$ state.

0.309e electron density from its 2s orbital, while the 2p orbital accepts 0.476e charges, tungsten donates 1.035e from its 6s orbital and it receives 0.301e in its 5d orbital. Consequently it can be rationalized that the formation of the W−C bonds is assisted by charge transfer from the 6s orbital of the tungsten atom to the 2s orbital of carbon and back transfer from C(2p) to W(6p) and W(5d) through the dative pπ−dπ and pπ-pπ bonds.

V. Conclusion

The potential energy surfaces of WC_2 were computed using the CASMCSCF followed by MRSDCI methods. The RCI technique was employed to include the spin−orbit effects for the electronic states of WC_2. Two nearly degenerate electronic states were found to be viable candidates for the ground state of WC_2, namely a high-spin $^5B_1$ state and a low-spin $^3A_2$ state with the latter becoming more stable at higher levels of theory. The equilibrium geometries of both states were found to be very acute isosceles triangles with the $^5B_1$ state exhibiting W−C bond lengths of 2.204 Å and C−W−C apex angle of 37.8°, while the equilibrium geometry of the $^3A_2$ state is W−C = 1.873 Å and 45.2° at the MRSDCI level in the absence of spin−orbit coupling. The spin−orbit splitting of the $^5B_1$ state is computed as 1875 cm^{-1}. The vibrational frequencies of the $^5B_1$ state are reported. The nature of bonding of the low-lying electronic states for WC_2 is discussed through the leading configurations, orbital compositions, and the Mulliken populations.

Acknowledgment. This research was supported by the U.S. Department of Energy under Grant DEFG02-86ER13558.

References and Notes

(1) Clemmer, D. E.; Shelimov, K. B.; Jarrold, M. F. *J. Am. Chem. Soc.* **1994**, *116*, 5971.
(2) Heath, J. R.; O'Brien, S. C.; Zhang Q.; Liu, Y.; Curl R. F.; Krato, H. W.; Tittel, F. K.; Smalley R. E. *J. Am. Chem. Soc.* **1985**, *107*, 7779.
(3) Cassady, C. J.; McElvany, S. W. *J. Am. Chem. Soc.* **1990**, *112*, 4788.
(4) Gingerich, K. A. *J. Less-Common Met.* **1985**, *110*, 41. Gingerich, K. A. *Curr. Top. Mater. Sci.* **1980**, *6*, 345.
(5) Gingerich, K. A.; I. Shim, I. In *Advances in Mass Spectroscopy 1985*; Todd, J. F. J., Ed.; Wiley: New York, 1986; p 1051.
(6) Pelino, M.; Haque, R.; Bencivenni, L.; Gingerich, K. A. *J. Chem. Phys.* **1988**, *88*, 6534.
(7) Pelino, M.; Gingerich, K. A.; Haque, R.; Bencivenni, L. *J. Phys. Chem.* **1986**, *90*, 4358.
(8) Shim, I.; Pelino, M.; Gingerich, K. A. *J. Chem. Phys.* **1992**, *97*, 9240.
(9) Shelimov, K. B.; Clemmer, D. E.; Jarrold, M. F. *J. Phys. Chem.* **1995**, *99*, 11376.
(10) Clemmer, D. E.; Shelimov, K. B.; Jarrold, M. F. *Nature* **1994**, *367*, 718.
(11) Shelimov, K. B.Clemmer, D. E.; Jarrold, M. F. *J. Phys. Chem.* **1994**, *98*, 12819.
(12) Simard, B.; Presunka, P. I.; Loock, H. P.; Berces, A.; Launila, O. *J. Chem. Phys.* **1997**, *107*, 307.
(13) Simard, B.; Hackett, P. A.; Balfour, W. J. *J. Chem. Phys.* **1997**, *107*, 307.
(14) Hamrick, Y. M.; Weltner, W., Jr. *J. Chem. Phys.* **1991**, *94*, 3371.
(15) Van Zee, R. J.; Bianchini, J. J.; Weltner, W., Jr. *Chem. Phys. Lett.* **1986**, *127*, 314.
(16) Weltner, W., Jr. *Magnetic Atoms and Molecules*; Dover Publications: New York, 1983.
(17) Roszak, S.; Balasubramanian, K. *J. Chem. Phys.* **1997**, *106*, 158
(18) Roszak, S.; Balasubramanian, K. *J. Phys. Chem.* **1997**, *101*, 2666.
(19) Roszak, S.; Balasubramanian, K. *Chem. Phys. Lett.* **1997**, *264*, 80.
(20) Roszak, S.; Balasubramanian, K. *Chem. Phys. Lett.* **1997**, *265*, 553.
(21) Majumdar, D.; Balasubramanian, K. *Chem. Phys. Lett.* **1997**, *280*, 212.

(22) Tan, H.; Liao, M. Z.; Balasubramanian, K. *Chem. Phys. Lett*. **1997**, *280*, 219.
(23) Tan, H.; Liao, M. Z.; Balasubramanian, K. *Chem. Phys. Lett*. **1997**, *280*, 423.
(24) Majumdar, D.; Balasubramanian, K. *Chem. Phys. Lett*. **1998**, *284*, 273.
(25) Shim, I.; Gingerich, K. A. *J. Chem. Phys.* **1982**, *76*, 3833.
(26) Shim, I.; Gingerich, K. A. *Surf. Sci.* **1985**, *156*, 623.
(27) Shim, I.; Gingerich, K. A. *Int. J. Quantum Chem.* **1992**, *42*, 349.
(28) Shim, I.; Pelino, M.; Gingerich, K. A. *J. Chem. Phys.* **1992**, *97*, 9240.
(29) Pacchioni, G.; Koutecky, J.; Fantucci, P. *Chem. Phys. Lett*. **1982**, *92*, 486.
(30) Russo, N.; Andzelm, J.; Salahub, D. R. *Chem. Phys.* **1987**, *114*, 331.
(31) Tan, H.; Dai, D.; Balasubramanian, K. *Chem. Phys. Lett.* **1998**, *286*, 375.
(32) Cartier, S. F.; May, M. B.; Castleman, A. W., Jr. *J. Am. Chem. Soc*. **1994**, *116*, 5295.
(33) McElvany, S. W.; Cassady, C. J. *J. Phys. Chem.* **1990**, *94*, 2057.
(34) Balasubramanain, K. *Relativistic Effects in Chemistry. Part A: Theory and Techniques*; Wiley-Interscience: New York, 1997; p 301. Balasubramanain, K. *Relativistic Effects in Chemistry. Part B: Applications*; Wiley-Interscience: New York, 1997; p 531.
(35) Ross, R. B.; Powers, J. M.; Atashroo, T.; Ermler, W. C. *J. Chem. Phys*. **1990**, *93*, 6654.
(36) Balasubramanian, K. *J. Chem. Phys.* **1988,** *89*, 5731.
(37) Pitzer, R. M.; Winter, N. W. *J. Phys. Chem.* **1988,** *92*, 3061.
(38) The major authors of ALCHEMY II are B. Lengsfield, B. Liu, and Y. Yoshmine
(39) Balasubramanian, K. *Chem. Phys. Lett.* **1986**, *127*, 585.
(40) Huber, K. P.; Herzberg, G. *Molecular Spectra and Molecular Structure IV, Constants of Diatomic Molecules*; Van Nostrand Reinhold: New York, 1979.
(41) Tan, H.; Liao, M. Z.; Balasubramanian, K. *J. Phys. Chem. A* **1998**, *102*, 6801.
(42) Pyykkö, P.; Tamm, T. J. *J. Phys. Chem. A* **1997**, *101*, 8107.
(43) Becke, A. D. Density-functional thermochemistry. III. The role of exact exchange. *J. Chem. Phys.* **1993**, *98*, 5648.
(44) Frisch, M. J.; Trucks, G. W.; Schlegel, H. B.; Scuseria, G. E.; Robb, M. A.; Cheeseman, J. R.; Zakrzewski, V. G.; Montgomery, J. A., Jr.; Stratmann, R. E.; Burant, J. C.; Dapprich, S.; Millam, J. M.; Daniels, A. D.; Kudin, K. N.; Strain, M. C.; Farkas, O.; Tomasi, J.; Barone, V.; Cossi, M.; Cammi, R.; Mennucci, B.; Pomelli, C.; Adamo, C.; Clifford, S.; Ochterski, J.; Petersson, G. A.; Ayala, P. Y.; Cui, Q.; Morokuma, K.; Malick, D. K.; Rabuck, A. D.; Raghavachari, K.; Foresman, J. B.; Cioslowski, J.; Ortiz, J. V.; Baboul, A. G.; Stefanov, B. B.; Liu, G.; Liashenko, A.; Piskorz, P.; Komaromi, I.; Gomperts, R.; Martin, R. L.; Fox, D. J.; Keith, T.; Al-Laham, M. A.; Peng, C. Y.; Nanayakkara, A.; Gonzalez, C.; Challacombe, M.; Gill, P. M. W.; Johnson, B.; Chen, W.; Wong, M. W.; Andres, J. L.; Gonzalez, C.; Head-Gordon, M.; Replogle, E. S.; Pople, J. A. *Gaussian 98*, revision A.7; Gaussian, Inc.: Pittsburgh, PA, 1998.